Article

Effect of Laser Beam Profile on Rotating Lattice Single Crystal Growth in Sb₂S₃ Model Glass

Courtney Au-Yeung [1],[†] , Dmytro Savytskii [2],[†] , Keith Veenhuizen [3] , Volkmar Dierolf [1] and Himanshu Jain [2],*

[1] Physics Department, Lehigh University, Bethlehem, PA 18015, USA; coa214@lehigh.edu (C.A.-Y.); vod2@lehigh.edu (V.D.)
[2] Materials Science and Engineering Department, Lehigh University, Bethlehem, PA 18015, USA; dms411@lehigh.edu
[3] Physics Department, Lebanon Valley College, Annville, PA 17003, USA; veenhuiz@lvc.edu
* Correspondence: H.Jain@Lehigh.edu
† Co-first authors who contributed equally.

Abstract: Laser heating of chalcogenide glasses has successfully produced rotating lattice single crystals through a solid-solid transformation. To better understand the nature of complex, orientation-dependent lattice rotation, we designed heat profiles of the continuous wave laser by beam shaping, fabricated larger Sb₂S₃ crystal dots in Sb₂S₃ glass, and investigated the lattice rotation where the crystal could grow in all radial directions under a circular thermal gradient. The results show that the rate of lattice rotation is highly anisotropic and depends on crystallographic direction. The nature of this rotation is the same in crystals of different orientation relative to the surface. The growth directions that align with the slip planes show the highest rate of rotation and the rotation rate gradually decreases away from this direction. Additionally, the presence of multiple growth directions results in a complicated rotation system. We suggest that the growth front influences the density of dislocations introduced during growth under confinement and thus affects the lattice rotation rate in these crystals.

1. Introduction

Continuous wave (CW) laser irradiation is a spatially selective heating method which offers an opportunity to fabricate crystalline architectures in amorphous solids with glass-crystal interfaces under controlled conditions. These architectures can be up to several micrometers wide and of practically unlimited length [1–3]. In fact, an amorphous phase can be directly converted into a single crystal by the solid-solid transformation via space selective laser heating of glass [4]. Such crystallization via laser heating is a fundamentally different process than classic processes such as Czochralski, Bridgman, and float-zone techniques in which a crystal is grown from a seed by cooling a melt. By contrast, the former process begins with the formation of a stable nucleus, which then grows under confinement by the surrounding glass.

In 2016, we reported the first successful fabrication of Sb₂S₃ single crystal dots (0D), lines (1D) [5], and 2D structures [6] on the surface on Sb-S-I glasses by heating the glass from ambient to crystallization temperature (Tx) without melting. Electron back scatter diffraction (EBSD) mapping indicates that the crystal grows macroscopically, while the crystal lattice simultaneously rotates gradually about an axis that is parallel to the glass surface and normal to growth direction [5]. For single crystal lines, the growth direction is essentially the same as the laser scanning direction and therefore the direction of lattice rotation. The scanning X-ray microdiffraction (μSXRD) analysis of these rotating lattice single (RLS) crystals suggests that the lattice rotates similarly to a single crystal that

is plastically deformed although no stresses are applied during laser heating [5]. Very recently, direct observations under a transmission electron microscope (TEM) have shown the presence of unpaired edge dislocations either distributed randomly or organized to form structures resembling small-angle tilt boundaries [7]. These observations lend support for the dislocation-based mechanism of spherulitic crystal formation widely observed in nature [8–11].

It was found that when multiple 1D crystal lines are grown from a single seed, the lines display different rates of lattice rotation; these results suggest that the crystal seed orientation with respect to the growth direction may have an influence on the lattice rotation process [5]. Additionally, when fabricating 2D single crystal architectures, the growth direction is no longer strictly parallel to the direction of laser motion [6]. To fabricate these structures, two different protocols, 'stitching' and 'rastering', were designed and tested. Analysis of μSXRD Laue patterns for these 2D structures show that the rotation has a component along the direction of laser motion but also another one orthogonal to it. The size of the latter component depends on the extent of overlap between successive 1D-lines. These results suggest that the presence of a more complicated growth front changes the way dislocations are introduced and will result in a more complex lattice rotation.

When a crystal dot is formed, the heat profile of a normally incident Gaussian laser beam and corresponding crystallization growth front are expected to have a circular shape. A nucleus will form at the center of the heat profile near the surface, followed by radial crystal growth forming a hemisphere. However, the shape of the growing crystal deviates from this shape due to anisotropic crystal growth causing preferred growth directions. Controlling the beam profile along with the presence of a preferred growth direction will result in a deformed growth front, which could potentially affect the rate of lattice rotation in the crystal. To understand the influence of this changing beam profile on the morphology and lattice rotation characteristics of the resulting crystals, we studied crystallization while varying the shape of the laser beam, using a spatial light modulator to transform the beam into circular rings with varying diameters. The use of a conventional finely focused Gaussian laser beam limited the width of the single crystal architectures to ~5 μm. By using ring-shaped beam profiles, we also hoped to incease the ultimate width of single crystal architecture. These larger crystals will better display the effects of a radial heat profile that allows crystal growth in all directions on the rotating lattice. We examined crystals written on the surface of Sb_2S_3 glass via CW laser heating with EBSD. We have selected Sb_2S_3 crystals as the model system for this study because it has been investigated extensively for fabrication of single crystal architecture in glass and is one of the very few chalcogenide compositions that can be crystallized into a ferro- and piezo-electric, non-linear optical phase [4,12].

2. Materials and Methods

The stoichiometric Sb_2S_3 glass sample was prepared by the ampoule quenching method. The procedure for the preparation of the glass samples and fabrication of crystals has been described in detail in previous publications [12,13]. To fabricate the Sb_2S_3 crystals, a fiber-coupled 639 nm diode laser (LP639-SF70, ThorLabs) was used for crystallization. A spatial light modulator (SLM, LCOS-SLM, X10468 Series, Hamamatsu, Bridgewater, NJ, USA) was used to transform the beam profile from the original Gaussian distribution to rings of varying sizes. This "ring" procedure first induces nucleation as a dot using a circular beam profile. After the nucleation stage, the beam is transformed to rings of increasing diameter to induce growth at the edge of the crystal dot while minimizing any further changes in the center. At each growth stage, as the ring diameter increases, the power density within the ring is kept constant. The beam profiles in both the nucleation and growth stages utilize a uniform distribution of intensity, unlike the crystal in Figure 1 fabricated with a Gaussian intensity distribution. This implementation of "ring-shaped" heating profiles is described in detail in a previous publication [14].

The laser-irradiated regions were analyzed with a scanning electron microscope (SEM, 4300 SE, Hitachi, Clarksburg, MD, USA) in a water vapor environment to minimize the charging effects. Crystallinity and orientation of the crystal grains in laser-created dots were examined using the EBSD maps, in which Kikuchi patterns were collected by a Hikari detector inserted into the SEM specimen chamber. The step size for these maps was 0.2 μm with a hexagonal sampling grid. EBSD scans were collected and indexed using TSL (TexSEM Laboratory) orientation data collection and analysis software. All patterns were indexed using Sb_2S_3 crystal structure parameters. The diffraction patterns were indexed by a voting system and characterized by parameters such as the image quality (IQ) value votes, the fit-factor, and the confidence index (CI). The orientation imaging microscopy (OIM) software package (OIM Analysis, EDAX, Mahwah, NJ, USA) was used to identify crystal grains and generate crystal orientation deviation, inverse pole, and normal pole figure maps. For all EBSD results, the following values of Sb_2S_3 crystal lattice parameters of orthorhombic phase (space group Pbnm) were used successfully: a = 11.229 nm; b = 11.310 nm; and c = 0.3839 nm; further details can be found in a previous publication [4,5].

3. Results

Laser-fabricated Sb_2S_3 crystals are typically formed using a stationary laser beam with a Gaussian distribution of intensity where the nucleus forms at the center of the beam on the surface or just below the surface of the glass sample and then grows to become readily observable. An example of such a crystal can be seen in the SEM image in Figure 1a. The remaining panels of Figure 1 describe the nature of the lattice rotation in various directions of the so-formed elliptically shaped crystallized grain, which is established from a detailed analysis of the lattice orientation by EBSD mapping. Using TSL analysis software, inverse and standard pole figure maps were obtained as seen in Figures 1b and 1d, respectively. The inverse pole figure (IPF) displays a rather uniform purple color of the pixels indicating that a single crystal grain of Sb_2S_3 was produced. However, upon inspection the crystal orientation deviation (COD) map (Figure 1c) reveals a misorientation of up to 5° across the dot. Furthermore, the lattice rotation rate is greater (yellow-red in color) along the short axis than the long axis of the elliptical dot.

The details of how the orientation of the crystal lattice varies spatially throughout the crystal dot are obtained from the pole figure map (Figure 1d). A closer inspection of the [010] direction, which is most closely related to the crystallographic normal direction, provides further insight on this orientation variation. Each point on the pole figure map corresponds to a specific location on the crystal and represents its unique 3D crystal lattice orientation as a stereographic projection in 2D space for the scanned area of the crystal. The enlarged inset displays the orientation variation in closer detail. If there was no rotation of the crystal lattice, the pole figure would display a single dot, meaning a single orientation for the entire area. On the other hand, a wide distribution of points within the pole figure shows a large change in lattice orientation relative to pole figure direction across the crystal—in this case, a lattice rotation. On the pole figure map the blue points form an oblong shape with the shorter axis parallel to [100] and longer parallel to [001]. Overall, there is a smaller rotation (~3°) along [100] and larger (~5°) along the [001] projection. These directions are also displayed as arrows on the inverse pole figure map, Figure 1b, showing a correlation between the physical size of the crystal and extent of lattice rotation.

To reduce the anisotropic growth rate effect and to grow crystals from an initially formed dot seed radially outward, we used a spatial light modulator to modify the laser beam from its original Gaussian profile to rings of varying sizes. This investigation follows the same beam profile of rings of varying sizes as described in a recent publication [14], but the exposure times and laser power at each stage are different here than in the previous study, Figure 2. In this study, the power was reduced to 3 mW to induce single crystal formation by reducing the probability of forming multiple crystal grains found in the previous experiments. Additionally, the ramp time to reach the final power in each step was increased to gradually increase the power and allow for successful continued growth of

a single grain. This procedure increased the laser power at each step to maintain a constant power density throughout the entire crystallization procedure. With this procedure, we induced growth from the original crystal seed to fabricate in the end an approximately circular single crystal dot with a diameter of approximately 25 μm. Figure 3 shows images extracted from the video recorded in-situ during the laser-induced fabrication of the crystal dot. The results confirm radial growth of the crystal under laser beam heating at all the four stages.
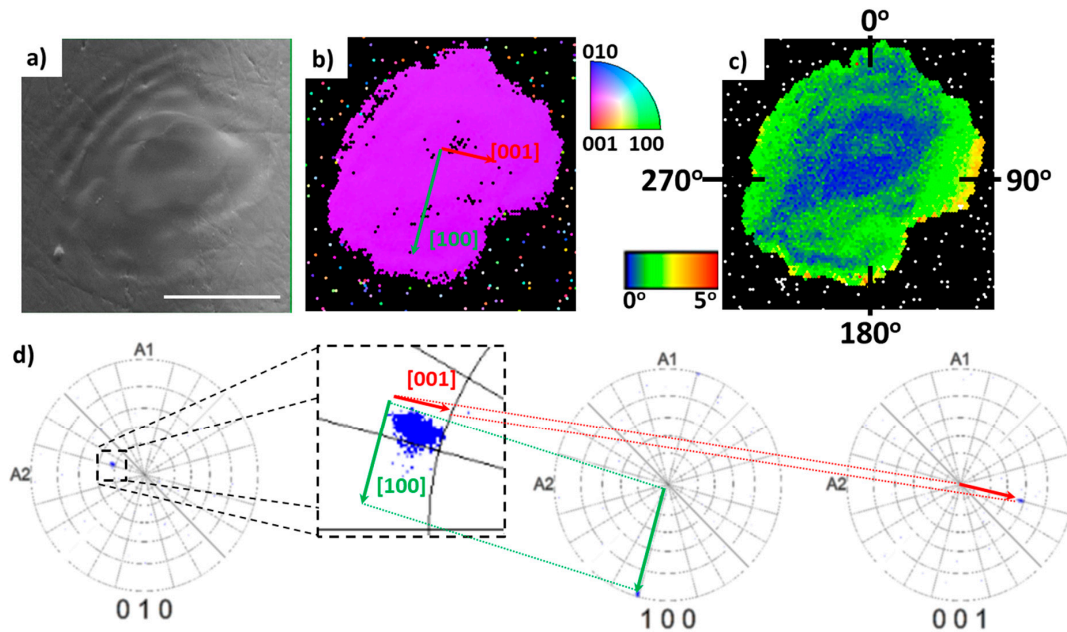

Figure 1. The single crystal dot induced by laser beam with Gaussian intensity distribution on the surface of Sb_2S_3 glass: (**a**) scanning electron microscope (SEM) image, (**b**) colored inverse pole figure (IPF) map with reference vector normal to sample surface (ND), (**c**) crystal orientation deviation (COD) map with reference to crystal orientation at the center of the dot, the marked numbers indicate positions along the crystal edges in degrees, and (**d**) pole figure (PF) maps in the (010), (100), and (001) crystallographic directions of the crystal dot. The inset represents an enlarged version of the (010) pole figure. The arrows on IPF (**b**) and PF (**d**) maps describe the direction of the lattice cell. The crystal was created by slowly ramping the power density from 0 to 2 mW in 5 s with time exposure 60 s in nitrogen environment. Scale bar corresponds to 4 μm.
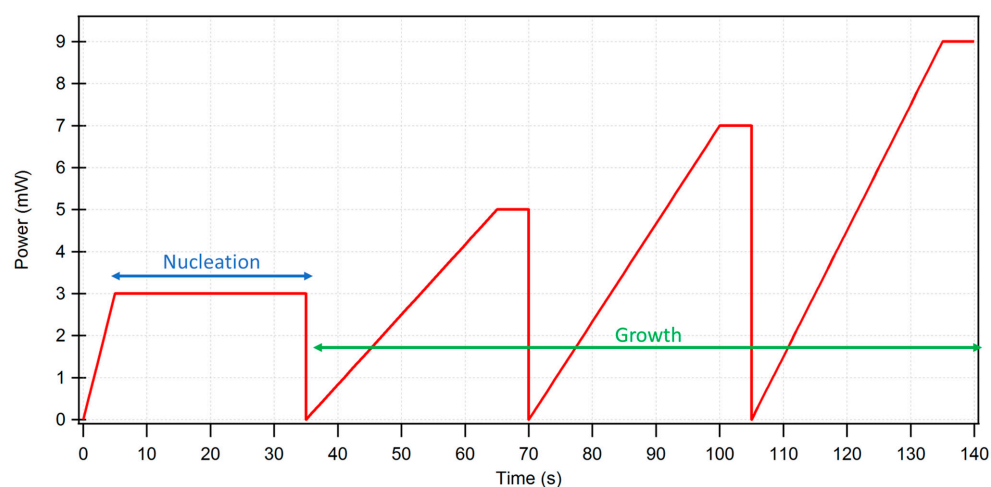

Figure 2. Heating schedule for dots created with a 'ring' procedure. The glass is illuminated with a circular beam of uniform intensity during the nucleation stage, designated in the figure, followed by 3 growth stages using rings of larger diameters. The power is increased to maintain a constant power density throughout crystallization.
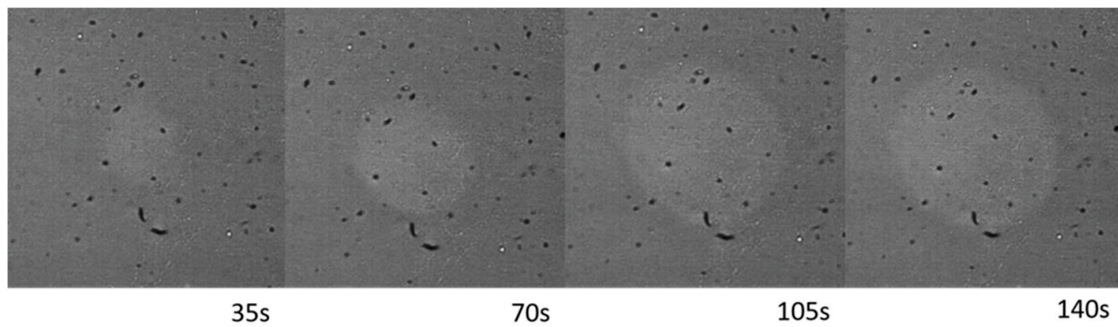
Figure 3. Time evolution of crystal growth on the surface of Sb_2S_3 glass. The numbers under images correspond to the time of exposure shown in Figure 2.

Following the "ring" laser heating protocol, the fabricated crystals were characterized using EBSD mapping. For two different crystal dots formed in this manner, the panels of Figures 4 and 5 describe the lattice including its rotation in various directions. Following the results of Figure 1, here we expected at the start of crystallization for a stable nucleus to form in the center of the dot and then begin to grow and rotate radially. To investigate this lattice rotation, the IPF, COD, and pole figure maps are plotted in the same fashion as for the crystal dot prepared by the laser with the Gaussian intensity profile in Figure 1. These SEM pictures show that a rounder Sb_2S_3 single crystal was produced under the ring laser profile in multiple ring-steps than the Gaussian profile in a single step. The IPF maps for these two crystals are essentially uniform in color indicating predominately single crystal (Figures 4b and 5b). However, the colors of the IPF maps are different, indicating different orientations of the crystal axes normal to the surface of the sample. Dot #1 (Figure 4) has a similar orientation as the dot shown in Figure 1. Similar to the dot induced by the Gaussian beam (Figure 1), this crystal also demonstrates the smallest rotation rates along positive and negative directions of the <100> and the highest rotation rates along the <001> (Figure 4c). From the pole figures (Figures 4d and 5d) we inspect closely the crystallography of the crystal growth process. Note that for the two non-normal directions, the middle and right pole figures, a single point is shown to represent the orientation of the entire crystal rather than displaying rotation observed along the normal direction in the panels in Figure 4a or Figure 5a. This representation increases the clarity of these directions and a more detailed structure for the pole figures for each crystal can be seen in the normal direction pole figure as well as the magnified inset. The maximum rotation rates for the dot shown in Figure 1 fabricated using the Gaussian beam, and the dots in Figures 4 and 5 fabricated using the ring-shaped laser beam protocol are 0.7, 1.1 and 1.3° per μm, respectively.

To further analyze this misorientation, and therefore the rotating lattice in crystallized structures fabricated by the ring laser heating protocol, line scans were taken from the origin to the edge of each crystal dot, starting at the top of the dot, referring to the vertical point marked by the arrow as the 0° position, and around the entire crystal clockwise. From these scans, we determined the rate of rotation in each direction and plotted the relationship between the rotation rate and position, as shown in Figure 6. Dot #1 has the highest rate of rotation, around 1.1° per μm, along the positive <001> direction and the smallest rate of rotation, around 0.2° per μm, along the positive <100> direction. For dot #2 (Figure 5) the minimal lattice rotation is observed along <100> projection, about 15° from the top of the crystal. In this case, the average rotation rate for the positive direction is close to zero. Dot #2 has the highest rotation rate (approximately 1.3° per μm) along the positive projection of the <010> crystallographic axis of Sb_2S_3 structure—100° from the top of the crystal. Although the maximum and minimum rotation rates were along different crystallographic directions, we find that the maximum and minimum rotations are approximately 90° from each other. For comparison, the "Gaussian" dot had a maximum rate of rotation around 0.7° per μm in the positive <001> direction and minimum value of 0.1° per μm in the negative <100> direction. These results show that overall the crystals

created with the ring-heating profile using SLM result in higher rates of rotation than in the traditionally laser-fabricated crystals with a Gaussian beam intensity.
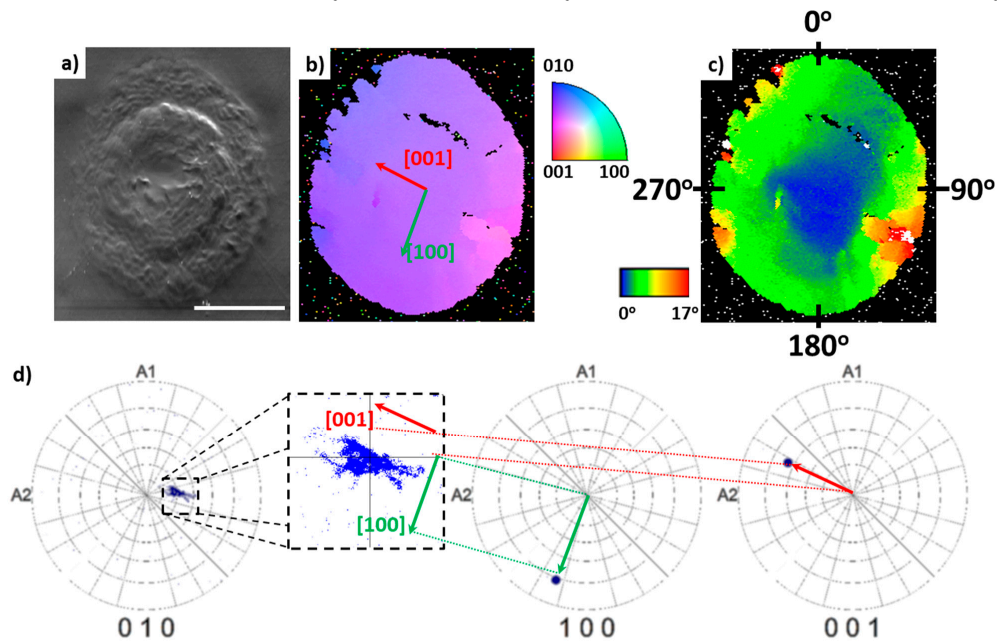

Figure 4. Sb_2S_3 single crystal dot #1 fabricated using 'ring' procedure on the surface of Sb_2S_3 glass: (**a**) SEM image, (**b**) colored inverse pole figure (IPF) map with reference vector normal to the sample surface (ND), (**c**) crystal orientation deviation (COD) map with reference to crystal orientation at the center of the dot, the marked numbers indicate positions along the crystal edges in degrees, and (**d**) pole figure (PF) maps in the (010), (100), and (001) crystallographic directions of the crystal dot. The inset represents an enlarged version of the (010) pole figure. The arrows on IPF (**b**) and PF (**d**) maps describe the direction of the lattice cell. Scale bar corresponds to 10 μm.
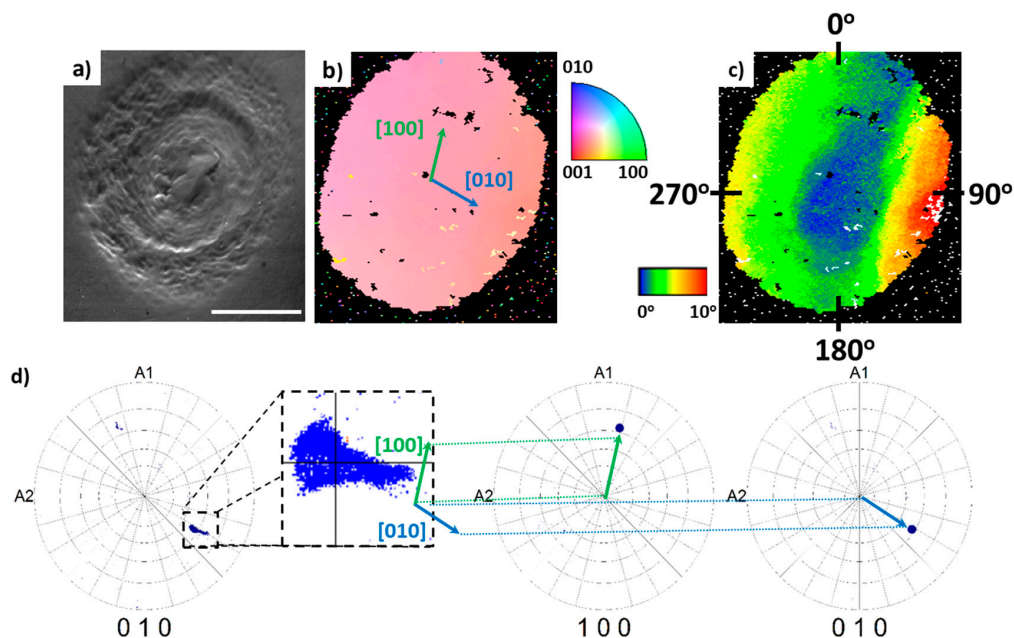
Figure 5. Sb_2S_3 single crystal dot #2 fabricated using 'ring' procedure on the surface of Sb_2S_3 glass: (**a**) SEM image, (**b**) colored inverse pole figure (IPF) map with reference vector normal to the sample surface (ND), (**c**) crystal orientation deviation (COD) map with reference to crystal orientation at the center of the dot, the marked numbers indicate positions along the crystal edges in degrees, and (**d**) pole figure (PF) maps in the (010), (100), and (001) crystallographic directions of the crystal dot. The inset represents an enlarged version of the (010) pole figure. The arrows on IPF (**b**) and PF (**d**) maps describe the direction of the lattice cell. Scale bar corresponds to 10 μm.
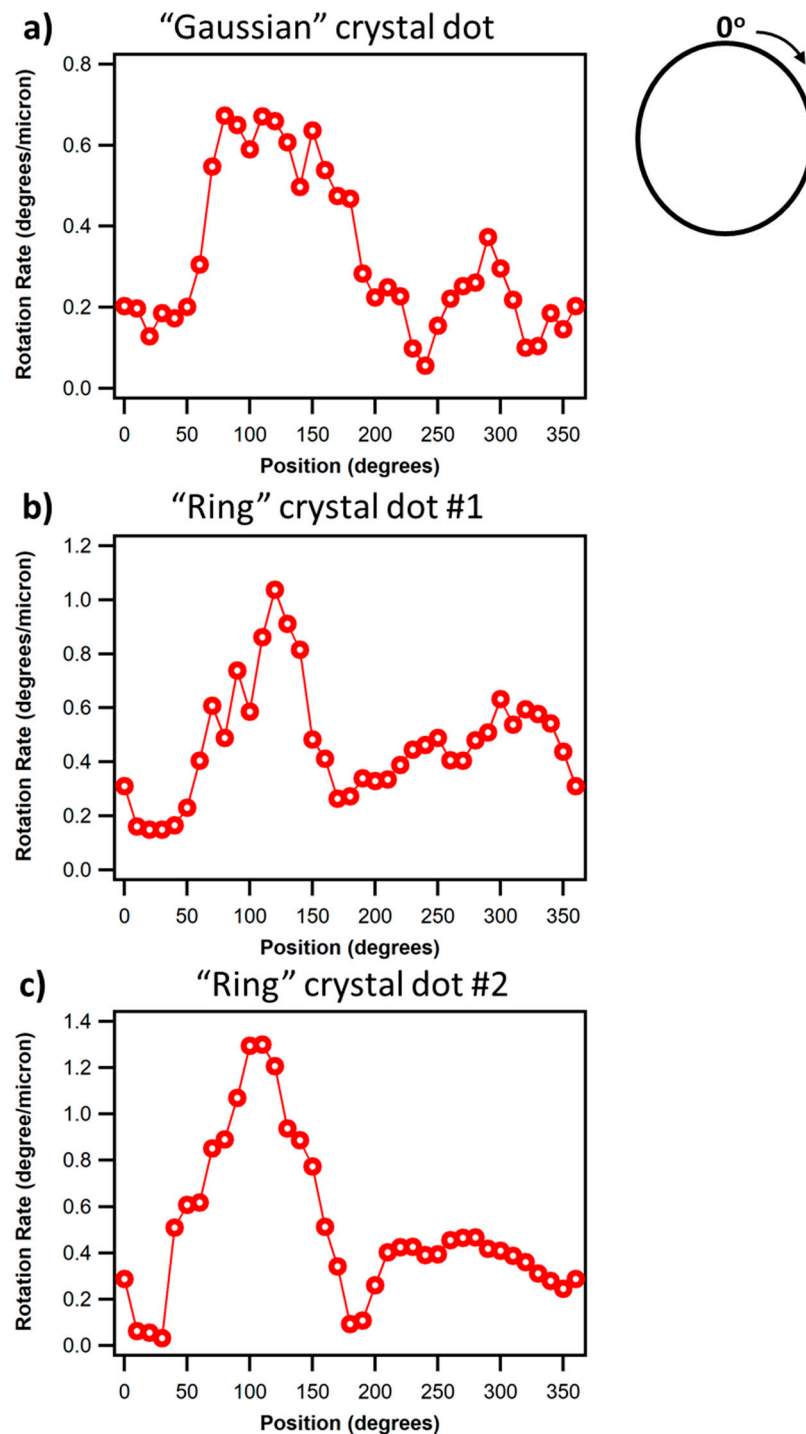
Figure 6. Graphs representing the rotation rate with respect to the position from the center to the periphery of the dot for (**a**) the "Gaussian" dot, and "ring" crystals #1 (**b**) and #2 (**c**). Here, 0° corresponds to the top of the crystal dot (as identified by the arrow in Figures 1, 4 and 5) and increases clockwise around the crystal structure, as seen in the schematic to the right.

Using single crystal dot #2 as an example, we observe that during the radial growth, the crystal lattice rotates radially, and the distribution of crystal lattice orientation forms a corresponding convex-like surface segment (Figure 7c,d). In other words, if we move radially from the center to the periphery of the dot, the orientation of the crystal lattice, for example, the (12 13 6) crystallographic plane that is parallel to the sample surface

in the center point of the dot, changes forming a convex surface. Our analysis of the spatial orientation of the crystal lattice shows that it rotates around tangentially oriented axes, which are normal to the radial growth directions. Figure 7b–d show the variation of orientation quantitatively, as well as the orientation of the crystal lattice for the two periphery and central points of the dot. The sign of the rotation depicted in Figure 7 was obtained from the EBSD maps in Figure 5. The crystal lattice rotates downward when we move from center to periphery of the dot as shown on Figure 7. Similar convex-like behavior of lattice rotation was detected for crystal dot #1 (Figure 4).
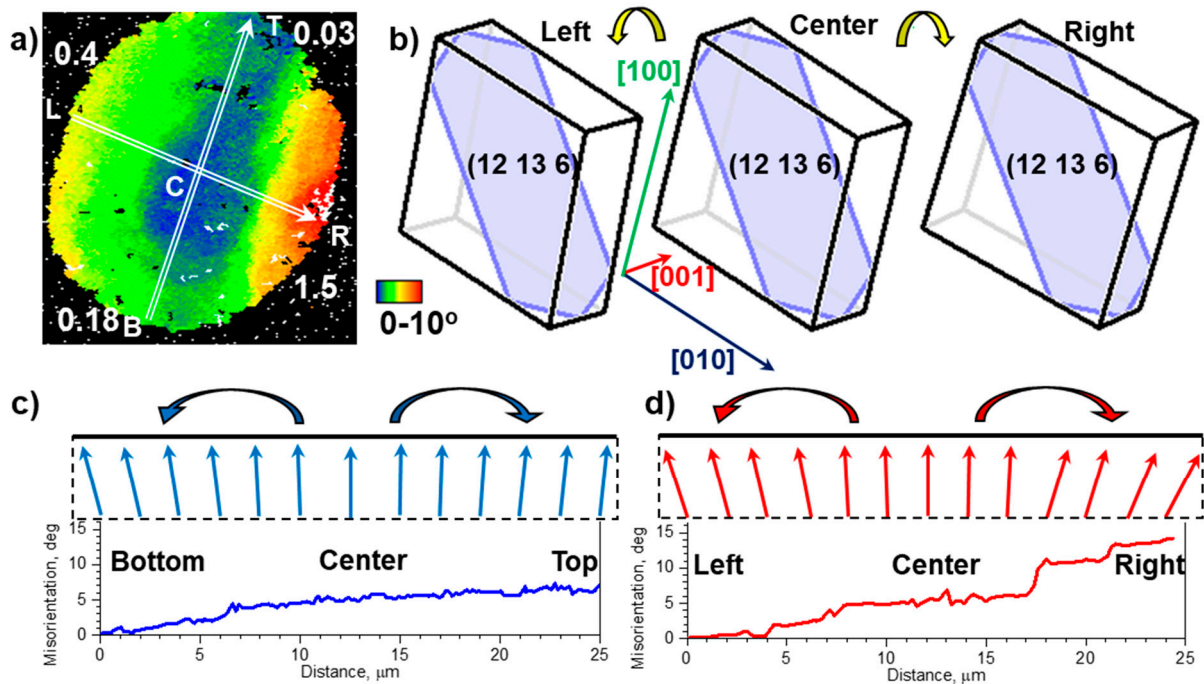

Figure 7. The orientational changes for single crystal dot #2 fabricated via the "ring" procedure. (**a**) Crystal orientation deviation (COD) map with reference to the crystal orientation at the center of the dot. Numbers in (**a**) indicate the average rotation rate (in degrees/μm) between the center of the dot (**C**) and corresponding periphery point indicated by the white lines for the top (**T**), bottom (**B**), left (**L**), and right (**R**) points of the crystal. (**b**) The crystal lattice orientation as it rotates as described by the yellow arrows. The plots (**c**,**d**) shows the misorientation profile that describes the misorientation of the lattice orientation between neighboring points from bottom to top (**c**) and left to right (**d**).

4. Discussion

The crystal in the laser-illuminated region by a Gaussian beam nucleates in the dot center where the temperature is the highest, and then grows in all directions from the center to the periphery. Similar to crystals formed as 1D lines [5,6], the growing crystal within a dot must also respond to change in density at the growth front. We then expect the introduction of unpaired dislocations to compensate for this density mismatch, which may order and produce tilt dislocation walls along the scanning direction [5,7]. It should be noted that growth rate and thermal conductivity of Sb_2S_3 are anisotropic, which can explain the resulting oblong crystal shape (Figure 1a). Additionally, in contrast to the growth of crystal lines along one laser scanning direction, the growth during fabrication of a crystal dot occurs along multiple inequivalent directions. Here, the lattice would rotate in response to the requirement of crystal growth in all radial directions in 2D (even 3D to some extent into the depth) starting at the dot center. The growth in multiple directions will result in a lattice rotation that is not along a single rotation axis seen in 1D single crystal lines with a relatively simple growth. With the lattice rotation occurring in multiple directions, several different spatially oriented dislocation systems are expected to occur

to facilitate this rotation. These dislocations may interact with each other creating a more complicated rotation within a crystal dot than in a line.

To keep the same conditions of crystallization while minimizing anisotropic influences, we used a "ring" heating protocol, which produces crystals through laser heating with a circular symmetric heat profile. The orientation perpendicular the surface for the "Gaussian" crystal in Figure 1 and dot #1 shown in Figure 4 is close to the (010) plane. For both crystals, we observed a similar anisotropy of the rotation rate, with the smallest rate of rotation along a projection of [100] and the highest along [001]. The crystals were formed through laser heating using beams with different shapes and intensity profiles, yet the character of the lattice rotation in 3D space is similar. Therefore, we infer that the rotation system is influenced by the radial crystal growth present in both the 'Gaussian' dot and the dots fabricated with the ring procedure. However, dot #2, also fabricated with the "ring" procedure, has a different lattice orientation and therefore may not be directly compared to the previous two crystals. Due to the uncontrolled process of nucleation, it is difficult to fabricate two crystals with identical spatial orientation. Nevertheless, this crystal also demonstrates anisotropy of the lattice rotation rate with a maximum along the projection of the [010] crystallographic direction. Although the crystals have different orientations, the anisotropic rates of rotation exhibit similar characteristics with a minimum along the longer length of the crystal and a maximum 90° from this length (Figure 6). Therefore, the growth front, which is the same in both cases, appears to have an effect on the lattice rotation. Recent observations have shown that dislocations primarily cause the lattice rotation in laser-crystallized Sb_2S_3 structures [7]. The results for the crystals fabricated through the ring procedure allow us to obtain additional insight about the complicated spatial behavior of the lattice rotation during radial growth. It has been found that the crystal lattice of Sb_2S_3 crystals can be distorted through the inclusion of dislocations to create spherulitic morphologies that depend on the growth front conditions [9]. We observe different rates of lattice rotation (from 0.03° up to 1.4° per μm) observed for the dots (Figure 6) along the radial directions suggesting that the anisotropy of the crystal structure, *namely* the orientation of dislocation slip systems in the crystal structure of Sb_2S_3 is an important parameter that controls the rotation of the lattice formed during crystal formation. Sokol et al. found that the Sb_2S_3 crystals have three possible dislocation slip systems [15]. Therefore, when the crystal is growing along these planes, we would expect an easier inclusion of dislocations and thus a higher rate of rotation [7]. During radial growth, we observed this increased rotation in both the positive and negative direction along these planes, approximately 90° and −90° from the top of the crystal dot. In the other growth directions, there would be a gradual decrease in the total dislocations as we move farther from the slip plane. This dislocation model explains consistently the anisotropic rates of rotation that we observe around the crystal structure. It is worth noting that we observe a band of minimum rotation close to the vertical direction in each crystal, although they have different orientations. We believe that the reason for this apparent coincidence is the existence of multiple slip systems in Sb_2S_3 [7]. As a result, different crystal orientations could result in a similar rotation rate configuration with the slip plane parallel to the direction of high dislocation density. As one moves away from this direction, fewer dislocations would be introduced. Then, perpendicular to the slip plane would result in the smallest density of dislocations and rotation, as observed here. Experimental parameters during irradiation, such as the laser polarization or non-normal incidence of laser beam relative to a local surface plane, can also assist in facilitating the anisotropic nature of the lattice rotation.

A similar lattice rotation was reported in the isothermal surface crystallization of cordierite from a non-stoichiometric composition $B_2O_3/Al_2O_3/MgO/SiO_2$ glass [16]. A crystal with only one nucleation center and no contact to neighboring crystals was selected for a 2D EBSD map. It showed a continuous change of orientation from the center to its outer boundary in all radial directions with an approximately isotropic rate of 0.34°/μm. The selected *c*-axis of cordierite was increasingly tilted upwards at 7° from the nucleation center to the periphery, in contrast to the downwards rotation observed

in our Sb_2S_3 crystals. The authors considered the incorporation of boron into the crystal structure of cordierite as an explanation of the observed orientational changes. In both cases, we found that defects within the crystal structure, in the inclusion of boron for these crystals and dislocations in our experiment, cause a rotation in the orientation throughout the crystal structure. Additionally, both cases present a rotation in all directions in the presence of radial growth.

5. Conclusions

In this work we have demonstrated a successful beam-shaping strategy for fabricating relatively large single crystal dots using a spatial light modulator. With regard to the nature of lattice rotation of such crystal dots we find that: (a) the direction of lattice rotation is specified by the direction of crystal growth, and (b) the rate of lattice rotation is determined by the direction of laser movement relative to lattice orientation. These observations confirm our previous conclusions on the lattice of single crystal lines fabricated by scanning the laser beam. When producing crystal dots using the "ring" procedure, the crystal growth is radial resulting in a complicated lattice rotation as compared to 1D lines. In dots, the lattice rotation rate is not constant, but varies from nearly zero to as high as 1.3° per μm in various growth directions.

In accordance with a recent study on laser fabrication of Sb_2S_3 RLS crystal in Sb-S-I glass [7], the lattice rotation observed here appears to occur due to the introduction of unpaired dislocations, which have higher density along the preferred slip directions on slip planes. For these planes, we observe a higher rate of rotation. In contrast, under this model the density of dislocations would decrease in directions away from slip planes, resulting in varying rates of rotation in different inequivalent directions. From a comparison of results on different crystal dots, we infer that the growth front has a larger effect on the rotating lattice compared to the starting nucleus orientation. In short, beam profiling using a spatial light modulator is shown to provide: (i) a mechanism of delineating the temporal and spatial temperature profiles, (ii) the ability to form crystals several times larger than possible with the Gaussian heat profile of typical lasers, and (iii) a method to engineer the rate of rotation in RLS crystals.

Author Contributions: Conceptualization, H.J and V.D; Methodology and Investigation, D.S., C.A.-Y., K.V; Formal Analysis, D.S., C.A.-Y., K.V.; Writing—Draft Presentation, C.A.-Y. and D.S.; Writing—Review and Editing, H.J. and V.D.; Funding Acquisition, H.J and V.D. All authors have read and agreed to the published version of the manuscript.

Conflicts of Interest: The authors declare no conflict of interest.

References

1. Honma, T.; Benino, Y.; Fujiwara, T.; Komatsu, T.; Sato, R. Technique for writing of nonlinear optical single-crystal lines in glass. *Appl. Phys. Lett.* **2003**, *83*, 2796–2798. [CrossRef]
2. Honma, T.; Benino, Y.; Fujiwara, T.; Komatsu, T.; Sato, R. Nonlinear optical crystal-line writing in glass by yttrium aluminum garnet laser irradiation. *Appl. Phys. Lett.* **2003**, *82*, 892–894. [CrossRef]
3. Honma, T.; Benino, Y.; Fujiwara, T.; Sato, R.; Komatsu, T. New optical nonlinear crystallized glasses and YAG laser-induced crystalline dot formation in rare-earth bismuth borate system. *Opt. Mater.* **2002**, *20*, 27–33. [CrossRef]
4. Savytskii, D.; Knorr, B.; Dierolf, V.; Jain, H. Demonstration of single crystal growth via solid-solid transformation of a glass. *Sci. Rep.* **2016**, *6*, 23324. [CrossRef]
5. Savytskii, D.; Jain, H.; Tamura, N.; Dierolf, V. Rotating lattice single crystal architecture on the surface of glass. *Sci. Rep.* **2016**, *6*, 36449. [CrossRef]
6. Savytskii, D.; Au-Yeung, C.; Dierolf, V.; Tamura, N.; Jain, H. Laser Fabrication of Two-Dimensional Rotating-Lattice Single Crystal. *Cryst. Growth Des.* **2017**, *17*, 1735–1746. [CrossRef]
7. Musterman, E.J.; Savytskii, D.; Dierolf, V.; Jain, H. The source of lattice rotation in rotating lattice single (RLS) crystals. *Scr. Mater.* **2021**, *193*, 22–26. [CrossRef]

8. Savytskii, D.; Dierolf, V.; Tamura, N.; Jain, H. Fabrication of single crystal architecture in Sb-S-I glass: Transition from dot to line. *J. Non-Cryst. Solids* **2017**, *501*, 43–48. [CrossRef]

9. Shtukenberg, A.G.; Punin, Y.O.; Gujral, A.; Kahr, B. Growth actuated bending and twisting of single crystals. *Angew. Chem. Int. Ed.* **2014**, *53*, 672–699. [CrossRef] [PubMed]

10. Shtukenberg, A.G.; Punin, Y.O.; Gunn, E.; Kahr, B. Spherulites. *Chem. Rev.* **2012**, *112*, 1805–1838. [CrossRef] [PubMed]

11. Lotz, B.; Cheng, S.Z.D. A critical assessment of unbalanced surface stresses as the mechanical origin of twisting and scrolling of polymer crystals. *Polymer* **2005**, *46*, 577–610. [CrossRef]

12. Savytskii, D.; Atwater, K.; Dierolf, V.; Jain, H. Formation of ferroelectric phases in Sb–S–I glasses. *J. Am. Ceram. Soc.* **2014**, *97*, 3458–3462. [CrossRef]

13. Savytskii, D.; Sanders, M.; Golovchak, R.; Knorr, B.; Dierolf, V.; Jain, H. Crystallization of stoichiometric SbSI glass. *J. Am. Ceram. Soc.* **2014**, *97*, 198–205. [CrossRef]

14. Au-Yeung, C.; Savytskii, D.; Veenhuizen, K.; Jain, H.; Dierolf, V. Polarization and surface effects on the seed orientation of laser induced Sb_2S_3 crystals on the surface of Sb-S-I glass. *Cryst. Growth Des.* **2020**, in press.

15. Sokol, A.A.; Kosevich, V.M.; Bagmut, A.G. Defect structure of Sb2S3 crystals revealed by electron microscope crystal lattice imaging techniques. In *Growth of Crystals*; Givargizov, E.I., Ed.; Springer: Boston, MA, USA, 1986; pp. 322–331, ISBN 978-1-4615-7121-6.

16. Wisniewski, W.; Baptista, C.A.; Rüssel, C. Orientational changes during the surface crystallisation of cordierite from a $B_2O_3/Al_2O_3/MgO/SiO_2$ glass. *CrystEngComm* **2012**, *14*, 5434–5440. [CrossRef]